RASĀYAN *J. Chem.*
Vol. 18 | No. 2 |1154-1162| April - June | 2025
ISSN: 0974-1496 | e-ISSN: 0976-0083 | CODEN: RJCABP
http://www.rasayanjournal.com
http://www.rasayanjournal.co.in

PREPARING ZnO/RGO NANO COMPOSITE THROUGH HYDROTHERMAL SYNTHESIS FOR THE REALM OF BIOCHEMISTRY

Ravi Kota[1], T. Narasimhulu[2,✉], Jaya Ranga Rao Prathipati[2], Sow Bhagyalakshmi Matcha[3], Y. V. Bhaskara Lakshmi[2], P.V.S.K. Phanidhar Varma[1], M. BonjuBabu[1], T. Nagakrishna[4] and Satheesh Ampolu[5]

[1]Sanketika Vidya Parishad Engineering College-AU, Visakhapatnam-530048, A. P., India
[2]Baba Institute of Technology and Sciences (A)-JNTUGV, Visakhapatnam-530048, A. P., India
[3]College of Engineering (A), JNTUGV, Vizianagaram-535003, A. P., India
[4]MRAGR-Government Polytechnic College, Vizianagaram-535002, A. P., India
[5]Centurion University of Technology and Management, Vizianagaram-535216, A. P., India
✉Corresponding author: narsim.223@gmail.com

ABSTRACT

In this study, we used several analytical techniques to investigate the thermal, morphological, and structural properties of a nanocomposite consisting of reduced graphene oxide (RGO) and zinc oxide (ZnO) that was synthesized hydrothermally. X-ray diffraction (XRD) revealed distinct peaks at 2θ = 10.6°, corresponding to graphene oxide (002) reflections. Interestingly, the major diffraction peaks of the ZnO/RGO composite matched those of pure ZnO, indicating that RGO did not alter ZnO's preferred orientations or produce new crystal orientations. Further characterization with Fourier-transform infrared spectroscopy (FTIR) indicated that the aromatic C=C group and the C=O group had peaks at 1717.5 cm-1 and 1586 cm-1, respectively. We determined that the broadband at 3235.5 cm-1 was caused by the hydroxyl (-OH) group. ZnO was successfully integrated into RGO sheets, allowing the formation of a pure ZnO/RGO nanocomposite based on energy-dispersive X-ray spectroscopy (EDS) elemental analysis. The reduced weight percentage of zinc in the composite compared to pure zinc oxide demonstrated acceptable integration. Thermogravimetric analysis (TGA) of ZnO and ZnO/RGO nanocomposites demonstrated mass loss between 100 and 250°C, which corresponds to hydrate molecules evaporating. The ZnO/RGO nanocomposite, in instance, has a band gap energy of 2.09 eV (591 nm), compared to 2.93 eV (423 nm) in pure ZnO. The Zn-O-C interaction in the ZnO/RGO composite resulted in greater absorption intensity in the visible region (591 nm) than pure ZnO (423 nm). This suggests that the composite structure brought novel optical properties.

Keywords: Hydrothermal Process, Nano-Composites, Dyes, Anti-Bacterial Activities.

RASĀYAN*J. Chem.*, Vol. 18, No. 2, 2025

INTRODUCTION

The growing threat to public health posed by increasing water pollution, caused by the influx of hazardous substances such as fungicides, pesticides, and organic dyes as a result of rapid industrialization and urbanization, highlights the critical need for a sensitive and user-friendly detection technique across multiple domains.[1,2]To address this serious issue, several solutions have been developed, with advanced oxidation processes (AOPs) emerging as a popular choice because oftheir simplicity, speed, affordability, and versatility. Adsorption of organic pollutants onto photocatalyst surfaces is a critical stage in AOPs, preparing the path for future oxidation. When exposed to light, AOPs can effectively convert aquatic

http://doi.org/10.31788/RJC.2025.1829152

contaminants into non-toxic compounds.[3] Semiconductors such as TiO_2, CuO, Fe_2O_3, SnO_2, and ZnO have been widely recognised as effective AOP photocatalysts. ZnO and its alloys are particularly being investigated for their ability to degrade pollutants.[4,5,6]ZnO, with a broad 3.37 eV band gap and remarkable electrical, optoelectronic, photochemical, and catalytic capabilities, has shown promise in catalytic processes, particularly in nanostructure form, due to its high catalytic activity and large surface area.[7]However, the difficulty of rapid electron-hole pair recombination limiting photocatalysis requires the introduction of other materials. Graphene oxide (GO) is a good alternative to inhibit this recombination.[8] The primary purpose of this research is to hydrothermally synthesize a ZnO/RGO nanocomposite that will be utilized to photocatalytically degrade Congo red (CR) and Eosin yellow (EY) dyes in the presence of visible light. Furthermore, the efficacy of the synthesized nanocomposite to inhibit Escherichia coli was investigated. ZnO/RGO nanocatalysts were produced hydrothermally, and the nanocomposite was thoroughly characterized using a variety of analytical techniques. The techniques used were photoluminescence spectroscopy (PL), transmission electron microscopy (TEM), UV-visible diffuse reflectance spectroscopy (UV-visible DRS), X-ray diffraction (XRD), and Fourier-transform infrared spectroscopy (FT-IR). These investigations enabled a better understanding of the optical and structural features of the produced nanocomposite. The photocatalytic activity of the CR and EY dyes was determined by measuring their degradation rates in response to visible light in the presence of the ZnO/RGO nanocomposite.

EXPERIMENTAL

Synthesis of Proposed Method

The usual synthesis technique involved mixing 50 mg of graphene oxide (GO) with a solution containing 10 mL of aqueous NaOH solution and 10 mL of 0.1 M zinc acetate. The resulting mixture was forcefully stirred for 30 minutes. The resultant slurries were then put into Teflon-lined autoclaves and exposed to hydrothermal heating at 180˚C for a day. After a thorough cleaning with water and ethanol, centrifugation was performed. Finally, the acquired product was completely dried in an oven overnight.

Characterization Techniques

X-Ray Diffraction

Figure-1 shows X-ray diffraction (XRD) patterns for GO, ZnO, and ZnO/RGO. Figure-1.1(b)[9] depicts the typical diffraction peaks at 2θ = 10.6°, which represent GO's (002) reflections. The XRD investigation shown in Fig.-1.1(c) reveals that the ZnO/RGO composite's principal diffraction peaks are quite similar to those of pure ZnO. Based on these similarities, it indicates that adding reduced graphene oxide (RGO) does not affect ZnO's preferred orientations or cause the development of new crystal orientations. Significantly, the XRD spectra of the ZnO/RGO combination include no additional diffraction peaks. This absence can be attributed to the intrinsic low diffraction strength of RGO, which is similar to findings published in other research studies.

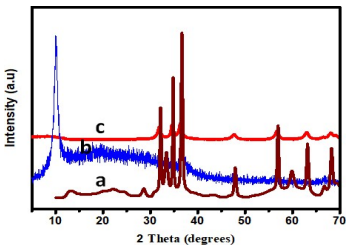

Fig.-1: XRD Patterns of (a) ZnO, (b) GO, and (c) ZnO/RGO

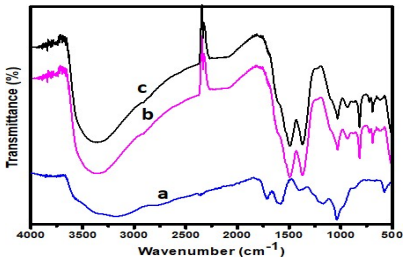

Fig. 2: (a) The ZnO/RGO, (b) GO, and (C) ZnO FTIR Spectra

FTIR Examination

FTIR spectroscopy was used to study the presence of oxygen-containing functionalities and the alterations caused by impregnation. Figure-2 (a) shows the FTIR spectrum of graphene oxide (GO), which includes peaks for the aromatic C=C group at 1717.5 cm^{-1} and the C=O group at 1586 cm-1. Furthermore, the wide band centered at 3235.5 cm^{-1} shows the existence of a hydroxyl (-OH) group.[12]The

FTIR spectra of the ZnO/RGO composite in Figure show a significant stretching vibration peak for Fe-O at 514 cm^{-1}, indicating the existence of metal oxide after hydrothermal treatment. Figure-2(b) Concurrently, the intensity of the C=O peak decreases, while the intensities of O-H and C-O decrease. These changes indicate that a component of the GO in the ZnO/RGO composite has been reduced, accompanied.

Analysis of FESEM-EDS

Fourier Emission Scanning Electron Microscopy (FESEM) was used to investigate the structural and anatomical features of the synthesized materials. Figure-4 shows the results of this research, with specific details about ZnO patterning on the surfaces of reduced graphene oxide (RGO) sheets revealed in Fig.-3(c) and (d). The introduction of ZnO causes exfoliation of RGO sheets, preserving their structural integrity and resulting in the hydrothermal synthesis of a composite material. Notably, the composite has lower ZnO content than pure ZnO. This size reduction is due to the large number of negatively charged sites formed by the interaction of positively charged Zn^{2+} sites, which are drawn to RGO sheets.[15]

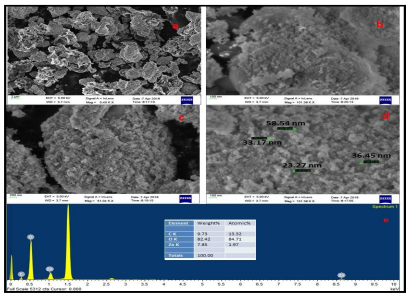

Fig.-3: FESEM and EDS Images of Prepared Samples

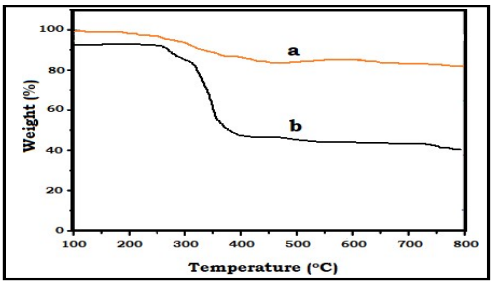

Fig.-4: TGA Curves of (a) ZnO and (b) ZnO/RGO

TG Analysis

Figure-4 shows the thermogravimetric analysis (TGA) curves for the ZnO/RGO composite. The sample was heated by airflow at a rate of 10°C per minute. The plots clearly illustrate that mass loss happens in the ZnO and ZnO/RGO nanocomposite at temperatures ranging from 100 to 250°C, which is due to the hydrate molecule. Interestingly, at approximately 370°C, there is a considerable mass loss, indicating pyrolysis of the carbon skeleton.[16] This observation demonstrates that reduced graphene oxide (RGO) was produced in the composite as a result of the reduction of the graphene oxide (GO) component.

Analysis of UV-DRS

Figure-5 shows the normalized UV-DRS spectra of ZnO/RGO composite and pure ZnO. The ZnO/RGO combination has a lower band gap value of 2.09 eV (591 nm), compared to pure ZnO's band gap energy of 2.93 eV (423 nm).[11] Notably, the ZnO/RGO mixture (591 nm) has higher absorption intensity and an absorption edge that shifts into a more visible range when compared to pure ZnO (423 nm). This boost is due to the Zn-O-C interaction in the ZnO/RGO composite. As a result, it can be confirmed that the combination of pure zinc oxide (ZnO) and reduced graphene oxide (RGO) has an excellent response to visible light, hence improving photocatalytic activity.

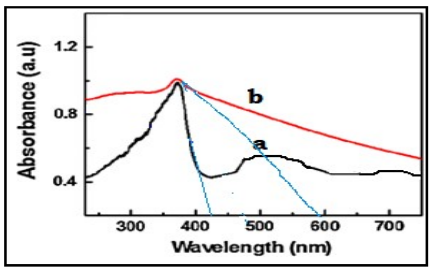

Fig.-5: UV-DRS Spectra of (a) ZnO and (b) ZnO/RGO Nanocomposite ZnO/RGO Photo Catalytic Degradation of CR

RESULTS AND DISCUSSION

The effects of exposure to visible light on the degradation of Congo red (CR) dye were investigated to assess the photo-catalytic efficiency of the synthesized ZnO/RGO composite. Maximize the reaction conditions, a thorough examination of several factors, including pH, catalyst quantity, and dye concentration in the solution, was carried out.

Effect of pH of Dye Solution

To investigate the first effects of pH, the liquids were adjusted to acidic (pH 3), neutral (pH 7), and basic (pH 10) conditions. Other parameters, such as the initial concentration of Congo red (CR) dye (5 ppm) and catalyst dose (0.05 g), remained unchanged during this phase. The results show that the solution's pH has a considerable impact on the heterogeneous photo process. Figure 6 shows a comparison of degradation rates at pH-3, pH-7, and pH-10, with pH-3 showing the highest percentage. The composite demonstrated degradation efficiencies of 93%, 51%, and 37% at pH levels of 3, 7, and 10, respectively. Lower pH levels, such as pH-3, promote the production of hydroxyl radicals (•OH). This increased reactivity of hydroxyl radicals on the catalyst's surface, which interacts with adsorbed molecules, adds to the observed differences in degradation efficiency across pH settings.

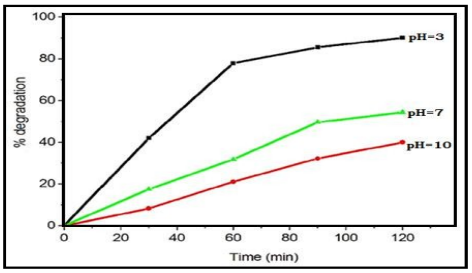

Fig.-6: pH's Impact on CR Dye Degradation

Catalyst Dosage's Effect

To analyze the impact of catalyst dose on Congo red (CR) degradation, several experiments were conducted to determine the optimal catalyst loading. While maintaining a constant pH of 3 and a dye concentration of 5 PPM for CR in an aqueous solution, the catalyst doses ranged from 0.05g to 0.05g. The degradation rate increased with the catalyst dosage, peaking at 0.05g.The degradation rate increased with the catalyst dosage, peaking at 0.05g. This impact can be due to the maintained active surface, which leads to greater dye adsorption in proportion to the increased number of catalyst molecules and, as a result, an increase in the number of photons absorbed. However, at a certain catalyst dose level, there is inadequate availability of dye molecules to accommodate the increasing number of catalyst molecules. As a result, degradation efficiency plateaus or declines, indicating a saturation point at which the excess catalyst no longer contributes to further CR breakdown via photo catalysis.

Catalyst Dosage's Effect

To analyze the impact of catalyst dose on Congo red (CR) degradation, several experiments were conducted to determine the optimal catalyst loading. While maintaining a constant pH of 3 and a dye concentration of 5 PPM for CR in an aqueous solution, the catalyst doses ranged from 0.05g to 0.05g. The degradation rate increased with the catalyst dosage, peaking at 0.05g. This impact can be due to the maintained active surface, which leads to greater dye adsorption in proportion to the increased number of catalyst molecules and, as a result, an increase in the number of photons absorbed. However, at a certain catalyst dose level, there is inadequate availability of dye molecules to accommodate the increasing number of catalyst molecules. As a result, degradation efficiency plateaus or declines, indicating a saturation point at which the excess catalyst no longer contributes to further CR breakdown via photo catalysis.

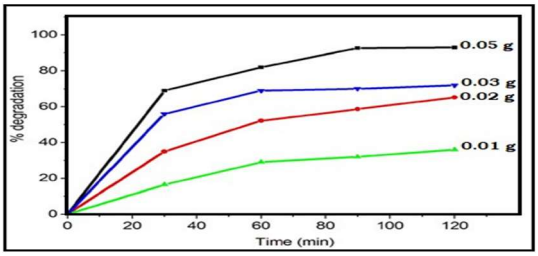

Fig.-7: Impact of Catalyst Dose on the Percentage of CR Degradation

Table-1: (%) Percentage Degradation of CR

Catalyst dose (g)	(%) Percentage Degradation of CR				Rate
	30min	60min	90min	120min	$mgL^{-1}min^{-1}$
0.05	67.33	80.19	90.11	93.06	2.5
0.03	52.63	66.70	66.70	70.89	2.3
0.02	26.03	44.39	57.22	67.14	1.20
0.01	15.79	23.36	28.58	30.87	0.69

Effect of Dye Initial Concentration

Table-2 and Figure 7 show how the initial concentration of Congo red (CR) affected the degrading efficiency of the nanocomposite ZnO/RGO. The impact of the starting CR concentration on the degradation rate was investigated at concentrations ranging from 5 to 25 parts per million, with the pH of the solution maintained at 3 and the chosen photocatalyst administered at a continuous dosage of 0.05 g. The photocatalytic degradation rate increased proportionally with the CR level, peaking at 25 ppm. However, above a certain level of extra dye, degradation efficiency began to deteriorate. This behaviour can be explained by the fact that increasing dye concentrations make more dye molecules available for excitation and energy transfer.

Table-2: Effect of Dye Concentration on the Percentage of CR that ZnO/RGO Breakdown

Dye Concentration (PPM)	(%) Percentage Degradation of CR			Rate order
	30min	60min	90min	$mgL^{-1}min^{-1}$
5	46.71	77.82	91	2.833
10	78.17	92.13	98	2.9636
15	47.88	71.39	83	1.8961
20	30.08	41.41	48	1.3818
25	9.33	28.36	30	0.0366

Photocatalytic Degradation of Eosin Yellow (EY)

Building upon the insights gained from the photocatalytic degradation of Congo red (CR), the investigation was further expanded to assess how well the composite degraded eosin yellow (EY) dye when exposed to visible light. Both pure ZnO and the ZnO/RGO composite were investigated in this context. Initially, ZnO had moderate photocatalytic activity against EY, leading to approximately 31% degradation after 120 minutes. As illustrated in Figure 8, the rate of EY solution degradation under acidic (pH 4) and basic (pH 10) conditions were investigated using the ZnO/RGO composite (50 mg). Figure 9 depicts solutions at pH-4 acidic and pH 10 basic conditions. The composite showed increased photocatalytic activity in the basic EY solution, with a degradation efficiency of 98% compared to 57% in the acidic solution. The maximum absorption wavelength of the EY dye solution (519 nm) transitioned to a colorless state when exposed to visible light and the ZnO/RGO composite. An initial dye concentration of 10 PPM, a catalyst dosage of 0.05g, and a pH value of 10 were identified as the optimal conditions for the ZnO/RGO composite in degrading EY. These results highlight the ZnO/RGO composite's potential for effective photocatalytic degradation under particular environmental circumstances. Because there were more impurity energy levels between the valence and conduction bands in the zinc oxide nanocomposite synthesized with decreased graphene oxide, it demonstrated higher

photocatalytic activity. This innovation minimizes the possibility of photogenerated holes and electrons recombining, making it easier for fresh electron-hole pairs to form. Reduced graphene oxide is a critical component that contributes to the effective suppression of defect bands[9], since it slows down the recombination process.

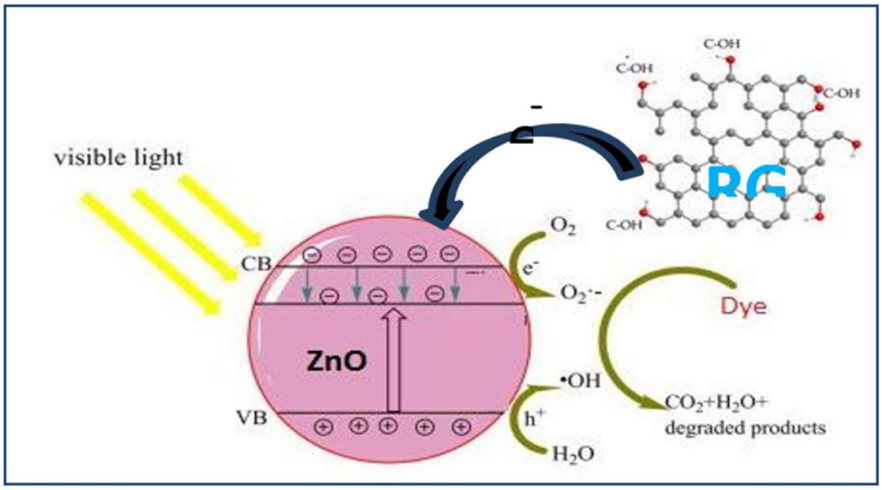

Fig.-8: ZnO/RGO Composite used for Photocatalysis to Degrade Dyes

Antimicrobial Activity

The ZnO/RGO photocatalyst demonstrated better effectiveness in photocatalytic activity assessments, which were principally measured using the Kirby-Bauer method in the disc diffusion test. Antibacterial activity experiments against *E. coli* were then performed utilising the previously stated photocatalyst and visible light. The bacteria were cultivated overnight, and the cells were properly diluted to form a cell suspension. In the antibacterial activity testing, a UV-filtering high-pressure mercury vapours lamp (400W Osram) was employed. Producing 35,000 lumens of visible light with an output range of 436-546 nm. To evaluate the antibacterial activity of the synthesized photocatalyst, a 4.9 mL aliquot of the *E. coli* cell suspension was pipetted into a laminar airflow chamber-sanitized petri dish.

Fig.-9: Schematic Representation of a Laminar Air Flow Chamber

After proper dilutions (10^-7) in sterile water, 1 mL aliquots of the solutions were applied onto petri dishes containing an Agar-Agar combination and incubated at 37 °C for 24 hours. Subsequently, the plates were scrutinized for zones denoting bacterial growth inhibition. The average inhibitory zone diameter in millimetres was used to assess the antibacterial activity of the drugs 27, 28, with the diameters of the inhibition zones[26] acting as markers. Inactive chemicals were characterized as those that lacked inhibitory zones. Zone Diameter Interpretative Standards and associated Minimum Inhibitory Concentration Breakpoints for

NCCLS M100-S12: Antimicrobial Susceptibility Performance Standards: The diameters of the zones of inhibition were determined through testing. The findings of sterilization studies revealed that visible light irradiation had no bactericidal effect on Figure 10a: (control A - no photocatalyst). In addition, two controls were tested: ZnO/RGO exposed to visible light for one hour (Figure 10b: control B) and a co-doped catalyst exposed to light irradiation in the dark for one hour (Figure 10c: control C). These two catalysts had no antibacterial activity at all. Antibacterial activity was observed in petri dishes containing ZnO/RGO when subjected to visible light. The photocatalyst's antibacterial activity began in 15 minutes and grew stronger as the exposure time increased. Figure 10 depicts the zones of inhibition, which are indicative of the nanomaterial's antibacterial properties. After being subjected to visible light irradiation, bacterial inactivation increased rapidly at fifteen-minute intervals. In this scenario, when exposed to visible light, the photocatalyst produces hydroxyl radicals. Reactive oxygen species (ROS), particularly hydroxyl radicals (•OH), are responsible for breaking down bacteria's outer membranes, which is why ZnO/RGO has antibacterial properties. This process leads to phospholipid peroxidation and, ultimately, cell death. When hydroxyl radicals are formed, they react with the peptidoglycan in the bacterial outer cell, acting as strong oxidizing agents. Using the disc diffusion method, the antibacterial activity of ZnO and ZnO/RGO against *E. coli* was evaluated. The results, as illustrated in Figure10, reveal a notable inhibition zone formed around the pleats, indicating the catalyst's effective inhibitory action. Figure 10 depicts the activity against *E. coli* at different time intervals: 15 min, 30 min, 45 min, and 60 min, respectively. In the absence of light (control A), ZnO and ZnO/RGO, the distance of the inhibition zone was 0 mm in the dark. However, upon exposure to artificial light, the zone of inhibition markedly increased at each 15-minute interval, measuring 5 mm, 6 mm, 8 mm, and 17 mm, respectively. Therefore, the zone of inhibition progressively increased with successive 15-minute intervals after the initial 15 minutes.

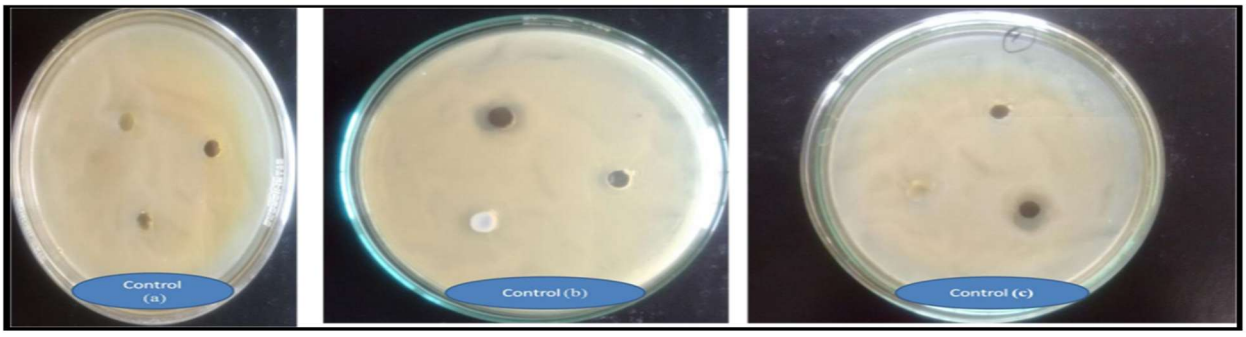

Fig.-10: Difference Controls for Antimicrobials

Photocatalytic Mechanism for the Photo Degradation of Dye Pollutants and Bacteria

The formation of hydroxyl radicals (•OH), which are required for colour degradation and antibacterial action, is mostly due to active catalyst particles. Here is a synopsis of the ZnO/RGO photocatalytic mechanism: Early in the •OH production process, the photocatalyst's antibacterial capabilities and photocatalytic removal of pollutants are inextricably linked. When visible light stimulates electrons in ZnO/RGO nanopowder to move into the conduction band, holes remain in the valence band. Recombining the generated electrons and holes is required to increase the catalyst's efficiency. During this stage, dopant ions absorb the produced electrons, preventing the ions from recombining.

$$ZnO + hv \rightarrow ZnO\ (h+) + ZnO\ (e-)$$

Holes create hydrogen ions and hydroxyl radicals when they come into contact with water adsorbed on ZnO/RGO or surface-bound hydroxyl groups.

$$ZnO(h^+)+H_2O \rightarrow ZnO+HO^{\bullet}+H^+$$

$$ZnO(h^+)+HO^- \rightarrow ZnO+HO^{\bullet}$$

The electrons are transferred to adsorb oxygen, producing superoxide anion,

$$ZnO/RGO(e^-)+O_2 \rightarrow ZnO/RGO+O_2^{\bullet -}$$

Following their interaction with the adsorbed water molecules, these superoxide anions produce peroxide radicals and hydroxyl ions.

$$ZnO/RGO(e^-)+O2^{\bullet -} +H_2O \rightarrow ZnO/RGO+HO_2^{\bullet}+HO^-$$

When peroxide radicals react with H+ to produce hydroxyl radicals and hydroxyl ions, hydrogen peroxide is produced as an intermediate product.

$$.ZnO/RGO(e^-)+HO2^{\bullet}+H^+ \rightarrow ZnO/RGO+H_2O_2ZnO/RGO(e^-)+H_2O_2 \rightarrow ZnO/RGO+HO^{\bullet}+HO^-$$

The holes oxidise these hydroxyl ions, resulting in the production of hydroxyl radicals. Every species involved thereby contributes to the creation of HO●. The adsorbed dye molecules then mix with the strong oxidant HO●, resulting in their breakdown.

$$.Dye + HO^{\bullet} \rightarrow Products$$

These hydroxyl ions are similarly oxidised by holes to produce hydroxyl radicals. Therefore, every species aids in the creation of HO●. The peptidoglycan on the outside of bacteria is reacted with and degraded by the potent oxidants HO●.

$$Bacteria + HO^{\bullet} \rightarrow Products$$

Thus, the formation of hydroxyl radicals and their role in photocatalytic activity play an essential role in the degradation mechanism.

CONCLUSION

In this section, we investigated the hydrothermal synthesis of ZnO/RGO nanocomposites and employed several experimental methods to investigate their thermal, morphological, and structural properties. The photocatalytic performance of the synthesized ZnO/RGO composite was evaluated using the degradation of Congo red (CR) and Eosin yellow (EY) dye. When exposed to visible light, the ZnO/RGO nanocomposite has higher photocatalytic activity, as evidenced by a comparison with ZnO experimental data. The composite had significant antibacterial activity against E. coli, demonstrating its potential as a robust antimicrobial agent.

ACKNOWLEDGMENTS

The nanotechnology lab at AU College of Engineering (A) provided the characterization studies, and the authors are grateful to the Inorganic Chemistry Laboratory at Andhra University in Visakhapatnam, India, for providing the synthesis facilities.

CONFLICT OF INTERESTS

The authors declare that there is no conflict of interest.

AUTHOR CONTRIBUTIONS

All the authors contributed significantly to this manuscript, participated in reviewing/editing and approved the final draft for publication. The research profile of the authors can be verified from their ORCID ids, given below:

K. Ravi http://orchid.org/0009-0005-5550-8914
T. Narasimhulu http://orchid.org/0000-0003-1519-0030
Jaya Ranga Rao Prathipati http://orchid.org/0000-0001-8561-1334
M. Sow Bhagyalakshmi http://orchid.org/0009-0004-3973-4498
Y.V. Bhaskar Lakshmihttp://orchid.org/0000-0002-8845-9224
P.V.S.K.PhanidharVarma http://orchid.org/0009-0002-2093
M. Bonju Babu http://orchid.org/0009-0008-3049-8416

T. Nagakrishna http://orchid.org/0009-0008-7067-3434
SatheeshAmpolu http://orchid.org/0000-0001-9191-3179

REFERENCES

1. M. R. Girish, K. M. Rakesh, B. K. Prashant, P. K. Pankaj, *Optical Materials*, **154**, 115720(2024), https://doi.org/10.1016/j.optmat.2024.115720
2. S. Hamed, Z. M. Mizwari, A. Rostaminia, H. Khojasteh, P. Aspoukeh and M. P. Mazhari, *Journal of Fluorescence*, **492**, 1(2024), https://doi.org/10.1007/s10895-024-04014-y
3. Matar, A. Hanan, A. Medhat, Ibrahim and M. El Hagary, *Diamond and Related Materials,* **133**, 109703(2023), https://doi.org/10.1016/j.diamond.2023.109703
4. Madi. K, Chebli. D, A. Youcef, H. Tahraoui, A. Bouguettoucha, M. Kebir, J. Zhang, Amrane, *Catalysts*, **14**, 62(2024), https://doi.org/10.3390/catal14010062
5. R. Sharma, H. Kumar, R. Kumari, G.Kumar, A.Dhayal, A.Yadav, D. Yadav, K. Yadav, Ch. Saini, Sal oni, A. Kumar, V. Pandit, *Results in Engineering, Elsevier BV*, **14**, 101161(2023), https://doi.org/10.1016/j.rineng.2023.101161
6. M. Ahamed, M. J. Akhtar, M. A. M. Khan, H. A. Alhadlaq, *International Journal of Nanomedicine*, **89**, 104(2021), https://doi.org/10.2147/IJN.S285392
7. S. Musmade, D. Hase, K. Kadam, G. Pandhare, K. Bhavsar, M. S. Khan, M. Rashid Khan, S. Gurav and V. Murade, *Journal of Inorganic and Organometallic Polymers and Materials*, **1**, 22(2024), https://doi.org/10.1007/s10904-024-03389-6
8. Zhu, Chunxiang, and X. Wang, *Nanomaterials*, **15(9)**, 682(2025), https://doi.org/10.3390/nano15090682
9. N. Elumalai, S. Prabhu, M. Selvaraj, S. Shanavas, M. Navaneethan, S. Harish, P. Ramu and R. Ramesh, *Journal of Materials Science: Materials in Electronics*, **32**, 28633(2021), https://doi.org/10.1007/s10854-021-07239-w
10. R. Abdullah, A.A. Jalil, M. Asmadi, N.S. Hassan, M.B. Bahari, M. Alhassan, N.M. Izzudin, M.H. Sa wal, R. Saravanan, H. K. Maleh, *International Journal of Hydrogen Energy,* **461**, 5(2024), https://doi.org/10.1016/j.ijhydene.2024.05.461
11. P. Kumar, M. C. Mathpal, G. K. Inwati, H.C. Swart, W.D. Roos, *Nanoscale Compound Semiconductors and their Optoelectronics Applications*, *Woodhead Publishing*, pp. 407-431(2022), https://doi.org/10.1016/B978-0-12-824062-5.00002-6
12. T. Azis, M. Z. Muzakkar, A. T. Nurwahida, N. Dali, L. O. A. Kadir, D. A. Lestari, L. O. A. Salim, *Journal of Oleo Science*, **72(12)**,1133(2023), https://doi.org/10.5650/jos.ess23152
13. Kaushal, Sandeep and R.Kumar, *Graphene-Based Photocatalysts: From Fundamentals to Applications. Chamistry: Springer Nature Switzerland*, **11**, 247(2024), https://doi.org/10.1007/978-3-031-66260-7_11
14. Balakumar, Vellaichamy, and R. Manivannan, *Metal oxides in nanocomposite-based electrochemical sensors for toxic chemicals,* pp. 263-292(2021), https://doi.org/10.1016/B978-0-12-820727-7.00005-7
15. G. Li, H. Liu, Z. Li, Y. He, M. Zhao, F. Chen, Ye Ma, M. Zhao, *Sensors and Actuators B: Chemical*, **420**, 136469(2024), https://doi.org/10.1016/j.snb.2024.136469
16. V. Jevtovic, A. U. Khan, Z. M. Almarhoon, K. Tahir, S. Latif, F. Abdulaziz, K. Albalawi, M. Zaki and V. Rakic, *Nanomaterials*, **13(4)**, 667(2023), https://doi.org/10.3390/nano13040667

[RJC-9152/2024]